In Situ X-Ray Absorption Spectroscopy Studies of Metal Hydride Electrodes

S. Mukerjee,* J. McBreen,* J. J. Reilly,* J. R. Johnson, and G. Adzic

Department of Applied Science, Brookhaven National Laboratory, Upton, New York 11973, USA

K. Petrov,* M. P. S. Kumar, W. Zhang, and S. Srinivasan*

Center for Electrochemical Systems and Hydrogen Research, Texas A&M University, College Station, Texas 77843, USA

ABSTRACT

In situ x-ray absorption spectroscopy (XAS) studies were done on three metal hydride electrodes, $LaNi_5$, $LaNi_{4.8}Sn_{0.2}$, $La_{0.8}Ce_{0.2}Ni_{4.8}Sn_{0.2}$, in 6*M* KOH. *Ex situ* measurements were also made on dry uncycled electrodes and on material from an $La_{0.8}Ce_{0.2}Ni_{4.8}Sn_{0.2}$ electrode that had been cycled 25 times. Comparison of the *in situ* XAS at the Ni K and at the La L_3 edge of charged and discharged electrodes indicates large changes in the electronic and structural characteristics on introduction of hydrogen. Results at the Ce L_3 edge in $La_{0.8}Ce_{0.2}Ni_{4.8}Sn_{0.2}$ show a transition from a mixed valent α to a γ-like Ce state as the lattice expands during charge. *Ex situ* x-ray absorption near-edge structures (XANES) at the Ni K edge indicate that the additions of either Ce or Sn fill empty Ni 3d states. The Ni K edge extended x-ray absorption fine structures (EXAFS) for all three alloys in the dry uncharged state were similar, indicating that minor substitutions for either the A or B component do not substantially change the structure. The Sn substitution causes an increase both in *a* and *c* axis as evidenced from increase in the Ni-Ni and the Ni-La distances. Partial substitution of La by Ce causes a slight contraction in the Ni-La distance. The Ni XANES and EXAFS indicate that about 6% of the Ni in the $La_{0.8}Ce_{0.2}Ni_{4.8}Sn_{0.2}$ corroded after 25 cycles. Ce XANES on the cycled electrode indicates some corrosion of Ce and the formation of Ce (III) state. The results indicate that XAS is a very useful technique for the study of alloy hydrides, particularly the role of electronic structure, the environment around minor constituents, and the corrosion of individual components.

Recent advances in the development of stable metal hydride alloy electrodes have led to their use as a replacement for cadmium anodes in rechargeable alkaline batteries.[1] Present battery electrodes are either AB_2 or AB_5 type alloys. The performance and life of these alloys greatly depend on their composition. In the case the AB_5 type alloys, substitution of either component in the prototype alloy, $LaNi_5$, with small amounts of other alloying elements can have major effects in the performance and stability of the alloy. Previous results with Ce, Sn, and Co substitution have demonstrated promising results in battery electrodes.[2] Recent results[3] have shown that Sn and Co substitution for some of the Ni causes a lowering of the hydrogen plateau pressure. Partial substitution of La with Ce results in improved corrosion resistance and cycle life. The Ce substitution also causes an increase in the hydrogen plateau pressure. An understanding of the mechanism of these effects would help in optimizing metal hydrides for various hydrogen storage and battery applications.

Most previous studies for understanding the role of various substituents in metal hydride alloys have focused on the structural aspects of such substitutions (via application of x-ray and neutron diffraction techniques). However, electronic effects, such as the role of empty d states are important for hydrogen storage.[4]

X-ray absorption spectroscopy (XAS) has the ability to probe *in situ,* both electronic (from the x-ray absorption near-edge structure, XANES) and geometric parameters (from the extended x-ray absorption fine structure, EXAFS) with element specificity. Most previous XAS studies on hydrides have been done in the gas phase. Tanaka *et al.*[5] and Lengeler and Zeller[6] did early XANES work on several metal hydrides. In the case of $NiH_{0.85}$, changes in the XANES on hydriding were attributed to changes in the density of empty p states.[6] Similar conclusions were made for $VH_{0.73}$.[5] Later Garcia *et al.* used both XANES and EXAFS to study the alloy hydrides $CeRu_2H_{3.75}$ and $CeFe_2H_{3.75}$ at the Ce L_3 edge and the Fe K edge.[7] More recently Suenobu *et al.* have done XAS studies on amorphous $LaNi_5$ thin films, involving gas-phase hydriding.[8, 9] Recently, an *in situ* XAS study on $LaNi_5$ electrode has been reported.[10]

The present study focuses on the application of *in situ* XAS to elucidate the electronic and geometric parameters as a result of (*i*) substitution of both A and B components of the prototype AB_5 alloy, $LaNi_5$, by Ce and Sn and (*ii*) the effect of charging and discharging the metal hydride electrode in 6*M* KOH.

Experimental

Alloy preparation and characterization.—All the alloys were prepared from high purity (>99.9%) starting components with the exception of Ce, which was of commercial purity. The alloys were prepared by an arc melting technique under He atmosphere. The melting procedure involved several remelting steps, each time followed by turning over the ingot. This was followed by an annealing step at a temperature of 1173K for 48 h, after which x-ray diffraction patterns were obtained for each alloy, and its lattice parameters determined.

The alloys were first characterized by obtaining the hydrogen pressure composition isotherms (PCT) in a modified Sievert's type apparatus according to the usual procedure.[11] This yielded the hydrogen plateau pressure and the hydrogen equilibrium storage capacity in the gas phase. The molar volume of hydrogen in the hydride phase was determined by comparing the lattice parameters of the hydrided and dehydrided phases using x-ray diffraction. The procedure for determining the lattice parameter and molar volume of hydrogen is given elsewhere.[12]

Electrochemical and cycling studies.—Electrochemical characterization measurements and cycling tests were made on electrodes prepared by pressing a mix, comprised of the alloy, carbon black (Vulcan XC-72), and 33 weight percent (w/o) PTFE binder (Teflon T-30), onto an 80 mesh nickel screen. The electrodes were tested for their initial capacity, charge-discharge characteristics, and cycle life in 6*M* KOH. The electrode potential was monitored using an Hg/HgO reference electrode and the capacities were measured to a cut of potential of −0.7 V. Cycle life was measured using a Bitrode battery cycler by charging at 0.5 C rate for 3 h and discharging at the same rate to a cutoff cell potential of 1.0 V *vs.* a nickel hydroxide counterelectrode. After cycling, the electrodes were washed to remove KOH. The active material was removed from the current collector, mixed with boron nitride (BN), and pressed into a pellet for XAS studies.

* Electrochemical Society Active Member.

Table I. Physicochemical properties of modified AB_5 type alloys.

Composition	Lattice Parameters a (Å)	Lattice Parameters c (Å)	Cell volume (Å^3)	Plateau pressure[a] atm	H_{max}/FU	V_H (Å^3)
$LaNi_5$	5.009	3.970	86.31	1.80	6.90	3.5[b]
$LaNi_{4.8}Sn_{0.2}$	5.056	4.019	88.96	1.01	6.26	3.2
$La_{0.8}Ce_{0.2}Ni_{4.8}Sn_{0.2}$	5.033	4.038	88.6	1.08	5.73	—

[a] All reported values are at a temperature of 299 K.
[b] Obtained from Ref. 35.

In situ XAS studies.—X-ray absorption spectroscopic (XAS) measurements were conducted at the beam lines X23A2 and X11 at the National Synchrotron Light Source (NSLS). Details of the monochromator design and energy resolution of the respective beam lines are given in detail elsewhere.[13-15] To eliminate second harmonics the beam was detuned by 15% at the Ni K edge and by 50% at the La and Ce L edges. *In situ* XAS measurements were made, in the transmission mode, at the La L_3, Ni K and Ce L_3 edges, at the end of charge and discharge. The electrodes for the *in situ* XAS measurements and for measurements on dry samples were thin disks (0.25 mm thick and 19 mm in diam) that comprised the alloy, carbon black (Vulcan XC-72), vitreous carbon fibers, and a polyvinylidine fluoride binder. They were prepared using a standard vacuum table paper making technique.[13] Prior to electrode fabrication, all the alloys were activated by subjecting each to several hydriding-dehydriding cycles in the Sievert's apparatus. This produces a fine powder with a Brunauer, Emmett, and Teller method (BET) surface area of ~0.5 m^2/gm, or a particle size of ~5 μm that eliminates thickness effects in the EXAFS and avoids the need for an electrochemical activation procedure. In the last dehydriding cycle the H content of the solids was measured by venting aliquots of desorbed H_2 gas into a measured volume; these values are listed in Table I. For detailed accounts of the activation procedure see Ref. 16 and 17. The separator was a single layer of a polyamide felt (0.125 mm thick) combined with a single layer of a 0.025 mm thick radiation grafted polyethylene separator. The counterelectrode was a 0.125 mm thick Grafoil disk. All components were soaked in 6*M* KOH and incorporated into a spectroelectrochemical cell that is described elsewhere.[13] The data acquisition for XAS comprised of three 12 in. ionization detectors (incidence I_o, transmittance I_t, reference I_{ref}). The reference channel was primarily for internal calibration of the edge positions and was used in conjunction with pure foils or oxide samples of the respective elements. For the Ni K edge pure N_2 was used in all the chambers, while for the La/Ce L_3 edges a mixture of 80% He and 20% N_2 was used in the incidence chamber while passing pure N_2 in the transmittance and reference chambers.

The metal hydride electrodes for the *in situ* studies were charged at a constant current of 1 mA for 16 h and discharged at a current of 2 mA to a potential of −0.5 V. The charging rate and time allowed for considerable overcharge because the electrodes contained only ≈50 mg of the alloy. XAS scans were run within 30 min of the termination of charge.

Data analysis.—The data analysis package used for the XANES analysis was the University of Washington analysis program.[18] The data analysis was done according to procedures described in detail elsewhere.[13-15,18-21] The EXAFS data analysis used computer algorithms developed by Koningsberger and co-workers.[18-21] The most comprehensive analysis of EXAFS was carried out on the data for dry uncycled electrodes at the Ni K edge. The Fourier filtering and analysis of the EXAFS spectra were conducted according to procedure described in detail elsewhere.[13-15,22] The windows for the forward and inverse Fourier transforms were chosen on the basis of nodes in the EXAFS in order to avoid excessive termination errors.[23] The slight variations in the Δk and Δr ranges, however, do not effect the outcome of the results.[23] The analysis was confined to the first major peak in the Fourier transform at 2.2 Å. Analysis of the EXAFS spectra for the alloys was done using one, two, three, and four shell fits using an iterative least square technique.[24] For fitting the sample data, phase and amplitude parameters derived from standard materials as well as those calculated using the University of Washington FEFF program (version 4.08) were employed.[25] The phase and amplitude parameters for Ni-Ni coordination shells were obtained from liquid N_2 data for a pure Ni foil (6 μm thick). The Ni-La and Ni-Sn phase and amplitude parameters were calculated theoretically using the FEFF program based on Cartesian coordinates input for the Wurtzite structure. The cell constants were varied to yield first shell bond distances that were equivalent to the sum of the atomic radii. In these theoretical calculations an S_o^2 value of 0.7 was used throughout.

Results and Discussion

X-ray diffraction, physicochemical, and electrochemical characterization.—Table I shows the results of x-ray diffraction analysis for the alloys. All the alloys were single phase and possessed the hexagonal $CaCu_5$ type (space group P6/mmm) structure, typical of the AB_5 type alloys. As indicated by the lattice parameters in Table I, substitution of B component (Ni) by Sn in the AB_5 metal hydride lattice ($LaNi_5$) results in an increase in the lattice parameters and, hence, the cell volume. However, substitution of the A component (La) with Ce causes a minor shrinkage along the *a* axis. The structural change due to partial substitution of Ni by Sn is reflected in the lowering of the hydrogen plateau pressure which improves the prospects for charging efficiency and charge retention of the hydride electrode. This structural change due to substitution is also reflected in a decrease in the gas-phase hydrogen storage capacity per formula unit (FU) and a reduced molar volume of hydrogen (V_H) The electrochemical performance characteristics of the metal hydride electrodes are given in Table II. The results indicate that substitution of Sn for Ni in the $LaNi_5$ lattice significantly improves the hydride stability. This is consistent with the reduction in the gas-phase hydrogen plateau pressure, and is in agreement with the recent results of Rathnakumar *et. al.*[26] The results in Table II indicate that these materials containing Sn or Ce give a very significant improvement in the cycle life relative to the $LaNi_5$. From these results it is clear that the substitution of the AB_5 type alloys with small amounts of

Table II. Performance characteristics of hydride electrodes with modified AB_5-type alloys.

Composition	Initial capacity (mAh/gh)	Discharge potential [mV(Hg/HgO)]	Rate capability 1C/3C[a] (%)	Decay rate (mAh/g cycle)
$LaNi_5$	350[b]	—	—	45%[b,c]
$LaNi_{4.8}Sn_{0.2}$	296	900	93	0.93
$La_{0.8}Ce_{0.2}Ni_{4.8}Sn_{0.2}$	315	935	83	0.77

[a] Ratio of capacity based on electrodes charged and discharged at C and C/3 rate, respectively.
[b] Obtained from Ref. 35.
[c] After 100 cycles.

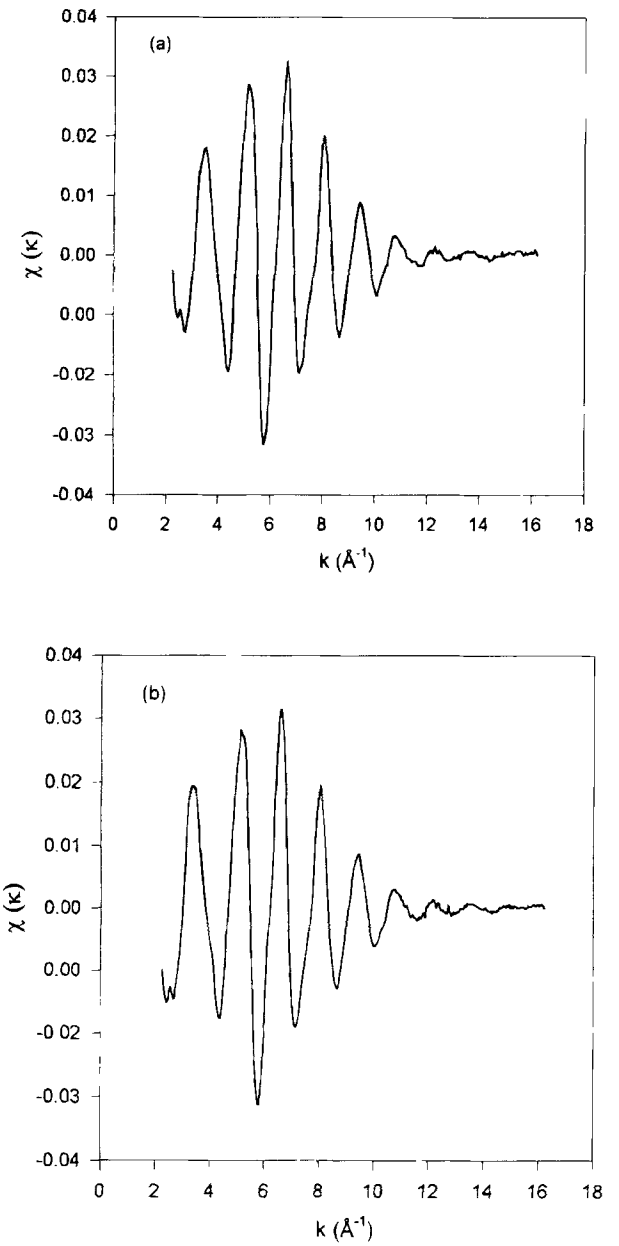

Fig. 1. Ni K edge EXAFS spectra for (a) $LaNi_5$ and (b) $LaNi_{4.8}Sn_{0.2}$ in dry uncharged electrodes.

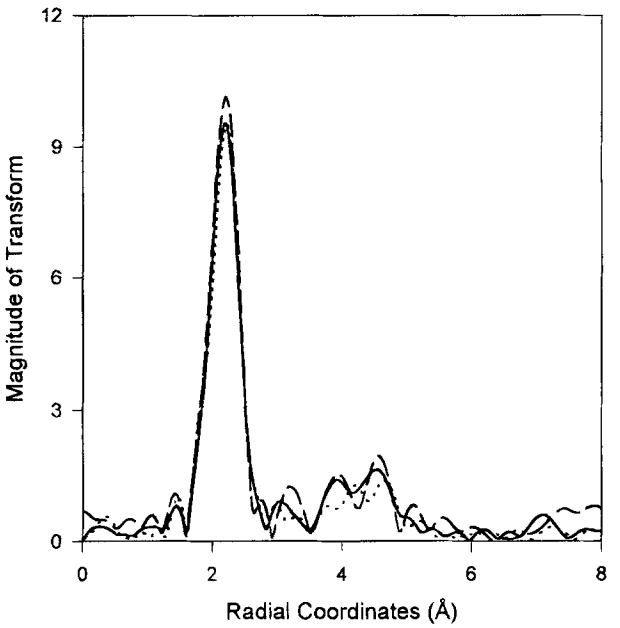

Fig. 2. Comparison of the Fourier transforms of the EXAFS (k^3 weighted) at the Ni K edge for $LaNi_5$ (—), $LaNi_{4.8}Sn_{0.2}$ (. . .), and $La_{0.8}Ce_{0.2}Ni_{4.8}Sn_{0.2}$. (- - -) in dry uncharged electrodes.

Sn and Ce causes significant changes in both gas-phase as well as the electrochemical characteristics of these alloys.

EXAFS results.—Figure 1 shows representative plots of the raw EXAFS data for $LaNi_5$ and $LaNi_{4.8}Sn_{0.2}$, respectively. Figure 2 shows a comparison of Fourier transforms of the EXAFS at the Ni K edge (Δk ranges in Table III) for the dry uncharged $LaNi_5$, $LaNi_{4.8}Sn_{0.2}$, and $La_{0.8}Ce_{0.2}Ni_{4.8}Sn_{0.2}$ electrodes. The results are almost identical. This is to be expected since all alloys have the hexagonal $CaCu_5$ structure. Detailed structural analysis using neutron diffraction show that there are two Ni sites, Ni_I and Ni_{II}, in $LaNi_5$.[27] The Ni_I atoms are in the basal plane (containing both Ni and La atoms) and are surrounded by six Ni_{II} atoms (three each above and below) at a distance of 2.461 Å. Within the basal plane each Ni_I is surrounded by three Ni_I atoms at a distance of 2.896 Å and three La atoms at a distance of 2.896 Å. The Ni_{II} exist in a plane that consists exclusively of Ni atoms and are surrounded by four Ni_I atoms at a distance of 2.461 Å, four Ni_{II} atoms at a distance of 2.508 Å and four La atoms at a distance of 3.202 Å. The changes induced by substituting Ce or Sn in the lattice are due mainly to changes in the backscattering amplitude from the Sn and distortions in the coordination symmetry. These apparently are minimal as evidenced from the Fourier transforms of the EXAFS shown in Fig. 2. The absence of an Ni-O contribution below 1.6 Å indicates that no significant oxidation of Ni occurred during electrode preparation.

Figure 3 shows that the substitution of Sn for some of the Ni causes a small change in the La L_{III} EXAFS. The Fourier transform window of the isolated EXAFS (Table III) was, however, limited in range due to the presence of La L_{II} edge, 400 eV beyond the L_{III} edge. In the case of $La_{0.8}Ce_{0.2}Ni_{4.8}Sn_{0.2}$, such an analysis was impossible because of the presence of the Ce L_{III} edge at 240 eV beyond the La L_{III} edge. In $LaNi_5$ each La atom is surrounded by six La atoms in the basal plane at a distance of 5.01 Å and two La atoms in the c direction at a distance of 3.98 Å. In addition each La atom is surrounded by six Ni_I atoms at a distance of 2.896 Å and twelve Ni_{II} atoms at a distance of 3.202 Å. The changes in the La EXAFS on the addition of Sn may be due to a reduction in the contribution of the Ni_{II} atoms because of the expansion along the c axis.[28] This could account for the shift in the peak to lower r values. Once again there is no evidence for any significant oxidation of the La during electrode preparation.

In order to obtain structural parameters as a function of Sn and Ce substitution a detailed EXAFS analysis was attempted at the Ni K edge for all the three alloys in their dry uncharged state. The windows in the k and r space used to obtain the corresponding forward and inverse Fourier transforms for the three samples as well as the reference standards are given in Table III and IV. The structure of $LaNi_5$ and the expected EXAFS phase shifts indicate that the inverse Fourier transform will contain contributions from three Ni-Ni and two Ni-La shells. These are listed in

Table III. Fourier transformation ranges of the forward and inverse transforms (k^3 weighted) at the Ni K edge for $LaNi_5$, $LaNi_{4.8}Sn_{0.2}$, and $La_{0.8}Ce_{0.2}Ni_{4.8}Sn_{0.2}$ as dry uncharged electrodes.

Composition	Δk (Å^{-1})	Δr (Å)
$LaNi_5$	3.10 to 14.56 (2.46 to 9.87)[a]	1.38 to 2.56
$LaNi_{4.8}Sn_{0.2}$	3.80 to 15.26 (2.45 to 9.87)[a]	1.40 to 2.86
$La_{0.8}Ce_{0.2}Ni_{4.8}Sn_{0.2}$	3.85 to 15.16	1.24 to 2.94

[a] Δk ranges for EXAFS data at the La L_{III} edge.

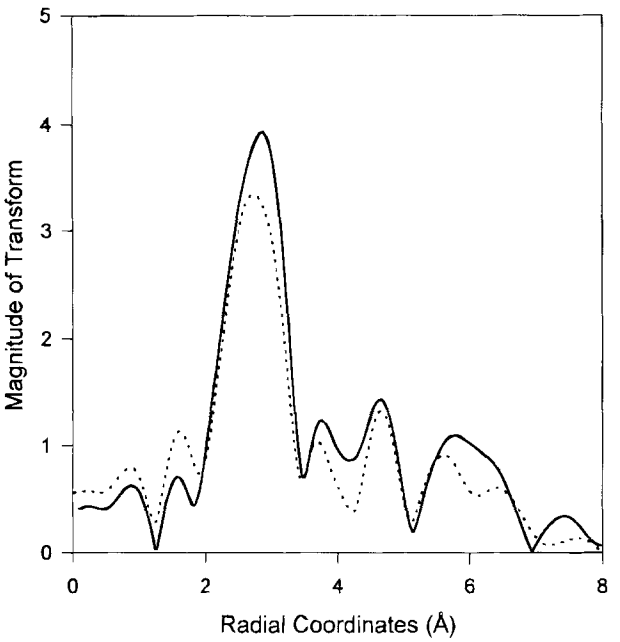

Fig. 3. Comparison of the Fourier transforms of the EXAFS (k^3 weighted) at the La L_{III} edge for $LaNi_5$ (—), and $LaNi_{4.8}Sn_{0.2}$ (. . .) in dry uncharged electrodes.

Table V. Unique solutions for the EXAFS analysis are impossible for a five-shell fit. Also in the case of the other alloys it is impossible to extract information on the Ni-Ce or Ni-Sn interactions. The best that can be expected is that the EXAFS analysis will give qualitative information on the effects of the addition of Sn and Ce. The approach taken was to fit the data to the simplest model that yielded a good fit. For all three alloys, the model consisted of two Ni-Ni and one Ni-La coordination shells. The result of the analysis is shown in Table VI. Figure 4 shows the representative plot for the three shell fit, in both k and r space for $LaNi_5$. The substitution of Sn for Ni causes an increase in all bond distances. This is consistent with the larger atomic radius for Sn (1.4 *vs.* 1.24 Å for Ni). The decreased Ni-La bond length for $La_{0.8}Ce_{0.2}Ni_{4.8}Sn_{0.2}$ is consistent with the smaller Ce atomic radius (1.72 *vs.* 1.88 Å for La). The increase in the Ni-Ni Debye-Waller factors for Sn containing alloys is consistent with the increases in bond lengths, and the disorder introduced by substituting Sn for Ni in the lattice. Similarly, the decrease in the Debye-Waller factor for the Ni-La interaction in $La_{0.8}Ce_{0.2}Ni_{4.8}Sn_{0.2}$ is consistent with the decrease in the Ni-La bond length. Thus the calculated parameters from the data analysis are internally consistent and are in agreement with the x-ray diffraction results (Table I). They also agree with previous x-ray and neutron diffraction results for $LaNi_5$ and $LaNi_{4.8}Sn_{0.2}$.[27,28]

A comparison of the results for $LaNi_5$ in Table VI with those in Table V indicates some uncertainty in the bond distances determined by EXAFS. For one- and two-shell fits R can normally be determined to within ±0.01 Å and N to within ±15%. In such complicated alloys the accuracies are reduced by at least a factor of three. The fact that the results of the substituted alloys could be fitted to a similar model indicates that it is unlikely that the substitution introduces any amorphous phases that cannot be detected by x-ray diffraction. It is also clear from the EXAFS that exposure of activated alloys to air does not result in any significant oxidation.

Table IV. Fourier transformation ranges of the forward and inverse transforms for the reference standards at the Ni K edge.

Reference standard	Δk (Å^{-1})	Δr (Å)	N_{ref}	R_{ref}
Ni-Ni standard Ni foil (liq. N_2 temp.)	3.45 to 15.24	1.10 to 2.80	12	2.49
Ni-La standard (FEFF Program)	3.05 to 19.95	1.50 to 2.50	4	3.50

Table V. Nickel coordination in $LaNi_5$.

Coordination shell	Coordination number (Normalized average)	Bond distance (Å)
Ni-Ni (1)	4.8	2.461
Ni-Ni (2)	2.4	2.508
Ni-Ni (3)	1.2	2.896
Ni-La (1)	1.2	2.896
Ni-La (2)	2.4	3.202

Significant changes occur in the Ni EXAFS during charge as shown by the representative plot for $LaNi_{4.8}Sn_{0.2}$ in Fig. 5. These changes are similar to those observed by Suenobu *et al.*, in the gas phase, for amorphous $LaNi_5$ films.[8,9]

Figure 6 shows a comparison of the Fourier transform of the Ni EXAFS for an uncycled dry $La_{0.8}Ce_{0.2}Ni_{4.8}Sn_{0.2}$ electrode and an electrode after 25 cycles, thus demonstrating the usefulness of the technique in detecting corrosion. The decrease in the peak at 2.0 Å and the appearance of a new peak at 1.5 Å indicates some corrosion of Ni to form $Ni(OH)_2$ for the electrode cycled 25 times (Δk = 2.83 to 15.60). Because of the contribution of several elements to the peak at 2.0 Å, phase correction techniques could not be used to separate the Ni-O contribution.[15] The data were analyzed by simply doing a backtransform (Δr = 0 to 1.6 Å), and using phase and amplitude parameters from a β-$Ni(OH)_2$ standard. This yielded an oxygen coordination number of 0.36 and an Ni-O bond distance of 1.96 Å, which is very close to that expected in $Ni(OH)_2$. In $Ni(OH)_2$ the coordination number is six. This indicates that about 6% of the Ni had corroded in 25 cycles. The result shows the power of the XAS technique to probe the corrosion of the alloy constituents because of its element specificity. No Ni corrosion products could be detected by x-ray diffraction presumably because of the amorphous nature of the $Ni(OH)_2$. Because of the complexity of the structure, the use of EXAFS in the study of major components in these alloys is of limited value. However, it is ideally suited for the study of environment around minor constituents. Furthermore, it is a very powerful technique for studying the corrosion of each of the individual components of the alloys during cycling. The XANES, however, yields very useful electronic information on the alloys.

XANES results at the Ni K-edge.—Figure 7 shows normalized Ni K edge XANES spectra for the three dry uncycled electrodes. The edge is shifted by about 1.5 eV below that found for Ni foil. Substitutions by Ce and Sn decrease the peak at 0.0 eV. Absorption at the K edge is due to the excitation of 1s electrons. Because of the selection rules only transitions into empty 4p states are dipole allowed. In systems with cubic or octahedral symmetry the weak quadrupole allowed transitions are observed as small pre-edge peaks in the XANES.[29] In the hexagonal symmetry of the alloys there is mixing of p and d states and as a result, transitions into empty p part of these mixed p-d states can

Table VI. Result of EXAFS analysis at the Ni K edge for $LaNi_5$, $LaNi_{4.8}Sn_{0.2}$, and $La_{0.8}Ce_{0.2}Ni_{4.8}Sn_{0.2}$ dry uncharged electrodes.

Composition	Coordination shell	EXAFS parameter N	R (Å)	$\Delta\sigma^2$ (Å^2)	ΔE_o (eV)
$LaNi_5$	Ni-Ni (1)	4.20	2.43	0.00200	−10.30
	Ni-Ni (2)	2.91	2.52	0.00008	−0.66
	Ni-La	2.63	3.17	0.01805	3.80
$LaNi_{4.8}Sn_{0.2}$	Ni-Ni (1)	4.80	2.50	0.00360	−2.15
	Ni-Ni (2)	4.00	2.74	0.01354	2.46
	Ni-La	3.10	3.35	0.00386	−4.35
$La_{0.8}Ce_{0.2}Ni_{4.8}Sn_{0.2}$	Ni-Ni (1)	4.30	2.50	0.00242	−4.95
	Ni-Ni (2)	4.15	2.76	0.01534	6.51
	Ni-La	1.42	3.13	−0.00617	−4.24

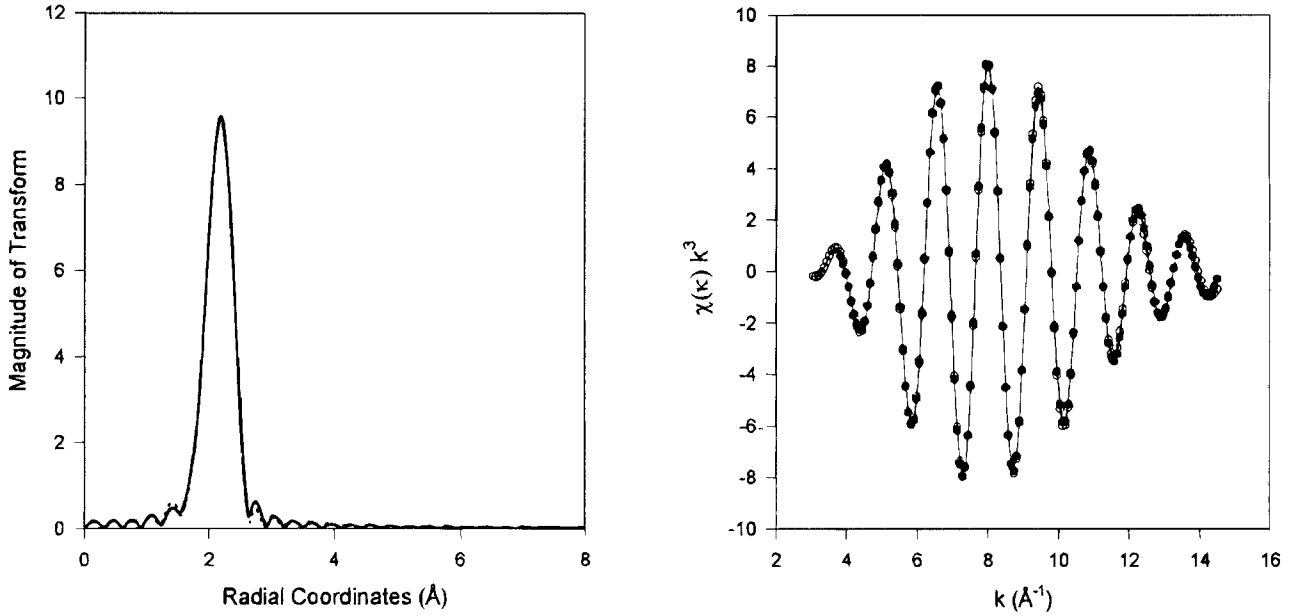

Fig. 4. A three-shell fit of Ni EXAFS (k^3 weighted) for $LaNi_5$ in (a, left) *r* space, (. . .) experimental data and (—) fit, and (b, right) *k* space, (○) experimental data, and (●) fit.

occur. Theoretical calculations of the density of states (DOS) by Gupta[30] have shown that the Fermi level of $LaNi_5$ falls in a rapidly decreasing portion of the Ni d bands which are not fully filled. Thus the intensity of the peak at 0.0 eV can be taken as an indirect measure of the number of empty Ni d states. The reduction in the intensity of this peak on the addition of Sn and Ce is due to either a partial filling of the Ni d states, a reduction in symmetry by lattice distortion, or both. Filling of the Ni d bands could account for the reduction in the hydrogen storage capacity and the decrease in the plateau pressure of the substituted $LaNi_5$ alloys.

Figures 8-10 compare *in situ* Ni XANES for the three alloys in the charged state with that found for the dry uncharged electrode. The data for the dry uncharged electrode and a discharged electrode in the cell were identical. The results are very similar to those found by Suenobu *et al.* for amorphous $LaNi_5$ films.[8,9] On hydriding, the Ni edge is shifted to coincide with that for the Ni foil. The theoretical calculations of Gupta[30] show that in $LaNi_5H_7$, the Ni d states are below the Fermi level and are narrowed. The mixed p-d states are no longer available for the excited 1s electrons, hence the shift in the edge on the ingress of hydrogen.

Figure 11 compares the Ni XANES for an uncycled $La_{0.8}Ce_{0.2}Ni_{4.8}Sn_{0.2}$, a cycled electrode, and for β-$Ni(OH)_2$. The appearance of a small white line in the cycled material signifies some Ni corrosion. A comparison of the area under the white line with that found for β-$Ni(OH)_2$ indicates that about 7% of the Ni has corroded. Thus, the results of the EXAFS and XANES are in good agreement.

XAS results at the La L_3 edge.—Figure 12 shows the effect of the alloying substituents on the La L_3 XANES. The addition of Sn and Sn combined with Ce causes considerable increases in the white line. The transitions at the La L_3

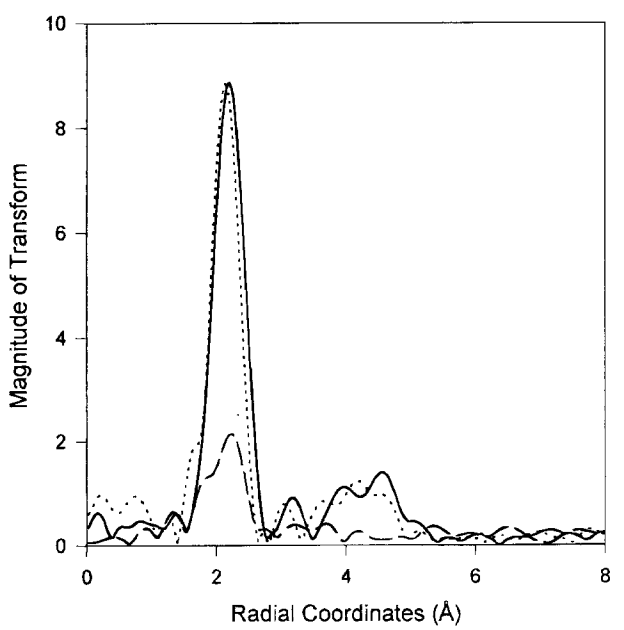

Fig. 5. Comparison of Fourier transforms of the EXAFS (k^3 weighted) at the Ni K edge for $LaNi_{4.8}Sn_{0.2}$ as a function of state of charge. $LaNi_{4.8}Sn_{0.2}$ dry *ex situ* uncharged (—), *in situ* charged (- - -), and *in situ* discharged (. . .).

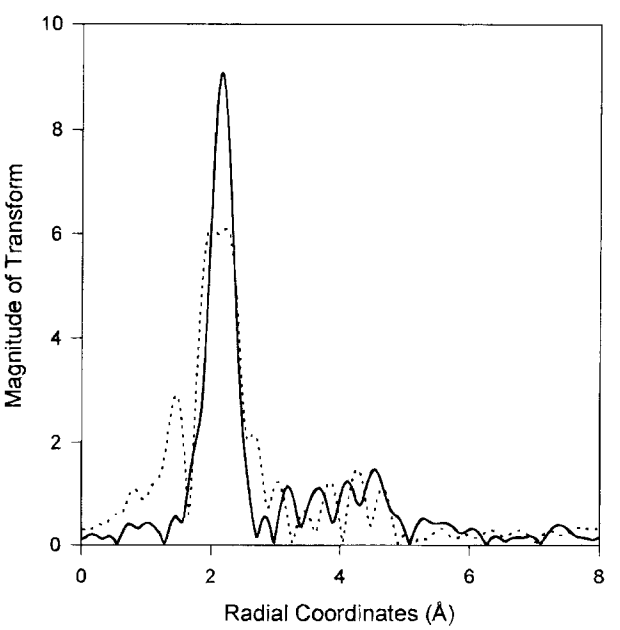

Fig. 6. Fourier transforms of the EXAFS (k^3 weighted) at the Ni K edge for $La_{0.8}Ce_{0.2}Ni_{4.8}Sn_{0.2}$. $La_{0.8}Ce_{0.2}Ni_{4.8}Sn_{0.2}$ dry uncharged electrode (—) and discharged (. . .) electrode after 25 cycles.

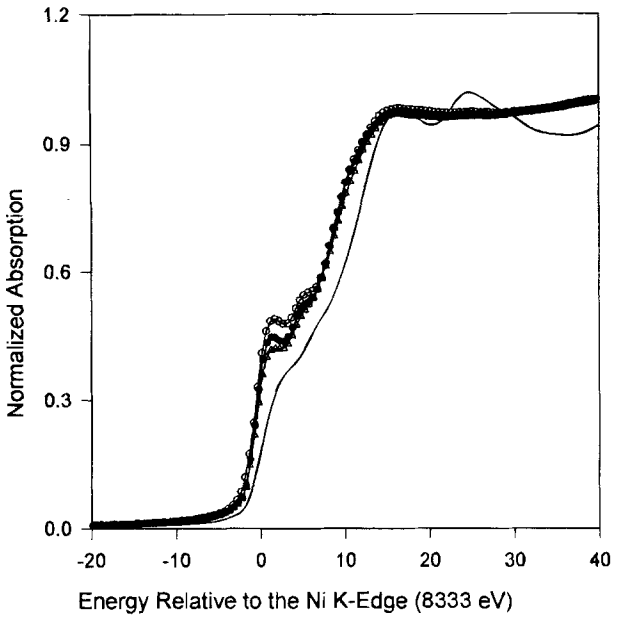

Fig. 7. Comparison of the Ni K edge XANES for $LaNi_5$ (○), $LaNi_{4.8}Sn_{0.2}$ (●), and $La_{0.8}Ce_{0.2}Ni_{4.8}Sn_{0.2}$ (△) in dry uncharged electrodes relative to the pure Ni foil (—) data.

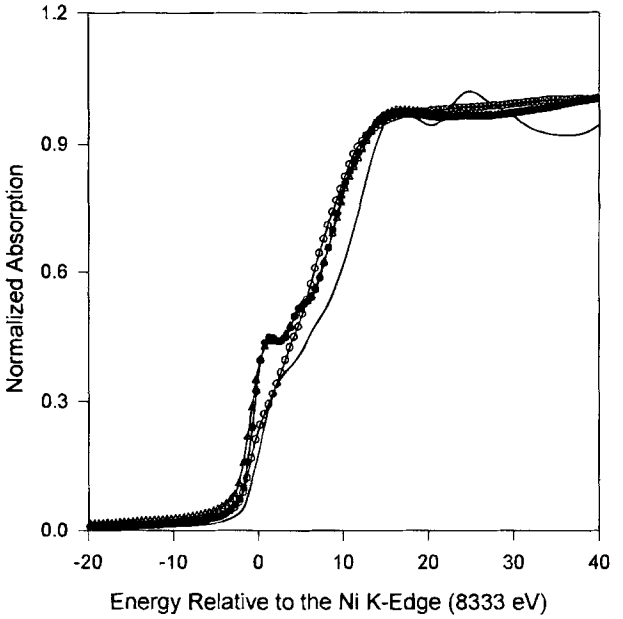

Fig. 9. Comparison of Ni K edge XANES spectra for $LaNi_{4.8}Sn_{0.2}$ as a function of state of charge. Ni foil (—), $LaNi_{4.8}Sn_{0.2}$ dry uncharged (●), *in situ* charged (○), and *in situ* discharged (△).

edge are due to the excitation of $2p_{3/2}$ into the La 5d states. Additions of Ce and Sn in the basal plane either increases the number of empty La d states or shifts their energy position with respect to the Fermi level.

Figures 13-15 show the *in situ* La L_3 edge XANES for the three metal hydride electrodes as a function of electrochemical hydriding and dehydriding. As evident from these figures, the electrochemical hydriding causes a further depletion in the La 5d orbital vacancy. This is evident from the increase in the magnitude of the white line as a result of hydriding. The calculations of Gupta showed that in $LaNi_5$ the nature of the d states at the Fermi level are largely nickel like with no lanthanum contribution.[30] However, her calculations show that in $LaNi_5H_7$ the DOS right above the Fermi level is mostly from the d orbitals of La. The present results support this conclusion.

In situ XAS results at the Ce L_3 edge.—Figure 16 shows that hydriding has remarkable effects on the Ce L_3 XANES for $La_{0.8}Ce_{0.2}Ni_{4.8}Sn_{0.2}$. This effect is similar to that observed by Garcia *et al.* for $CeRu_2$ and $CeFe_2$ in the gas phase.[7] Ce is unusual in that the energy of the inner 4f level is nearly the same as the outer 5d and 6s levels.[31] Thus small changes in energy and the environment around the Ce can change the relative occupancy of these atomic levels. This has been the subject of an enormous number of publications in the physics literature and several reviews.[31-33] At ambient temperature the two main allotropes are α-Ce and γ-Ce. Both have fcc structure with respective lattice constants of 4.83 and 5.15 Å. The γ-state has a $4f^15d^1$ configuration and the α-state has a mixed $4f^15d^1/4f^05d^2$ configuration. This is reflected in the Ce L_{III} XANES where γ-Ce has a spectrum similar to Ce (III) and α-Ce has a spectrum similar to Ce

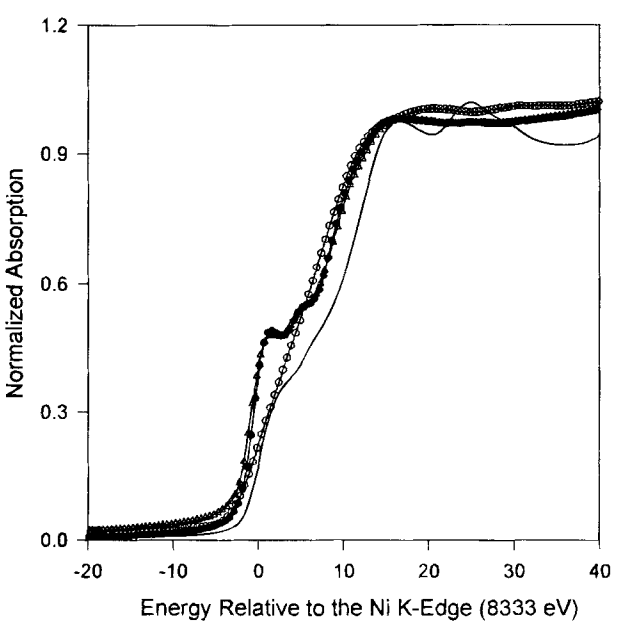

Fig. 8. Comparison of Ni K edge XANES spectra for $LaNi_5$ as a function of state of charge. Ni foil (—), $LaNi_5$ dry uncharged (●), *in situ* charged (○), and *in situ* discharged (△).

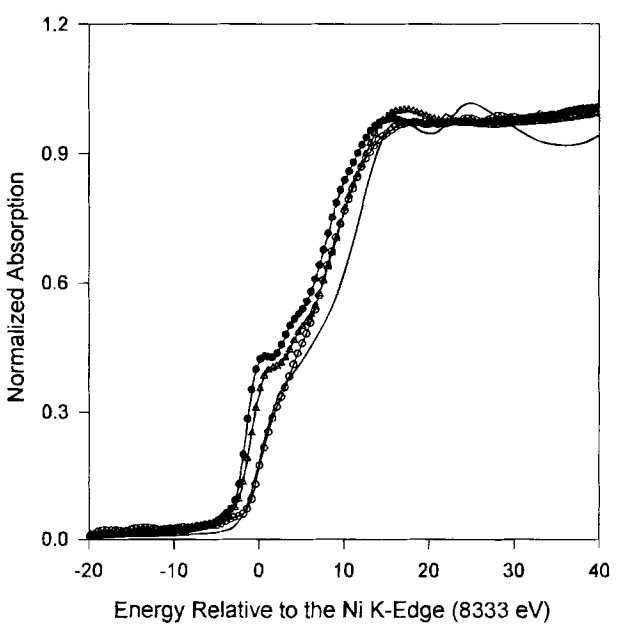

Fig. 10. Comparison of Ni K edge XANES spectra for $La_{0.8}Ce_{0.2}Ni_{4.8}Sn_{0.2}$ as a function of state of charge. Ni foil (—), $La_{0.8}Ce_{0.2}Ni_{4.8}Sn_{0.2}$ dry uncharged (●), *in situ* charged (○), and *in situ* discharged (△).

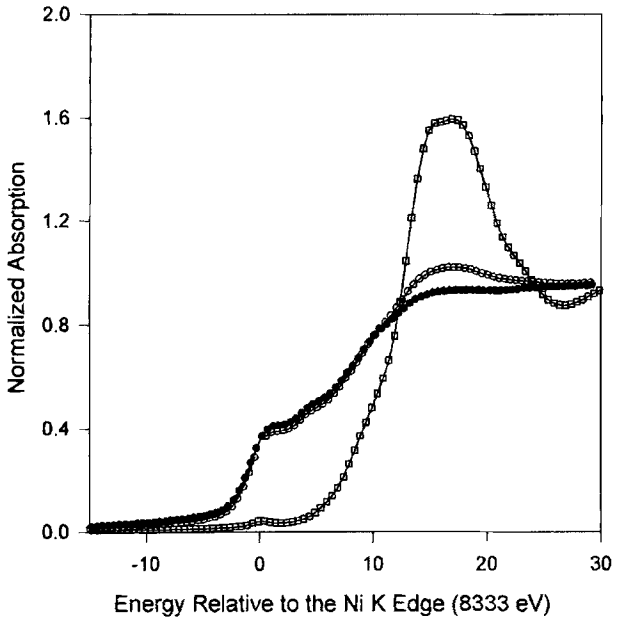

Fig. 11. Ni K edge XANES for $La_{0.8}Ce_{0.2}Ni_{4.8}Sn_{0.2}$ electrodes. $La_{0.8}Ce_{0.2}Ni_{4.8}Sn_{0.2}$ dry uncharged (●), *ex situ* discharged after 25 cycles (○), and a β-$Ni(OH)_2$ reference standard (□).

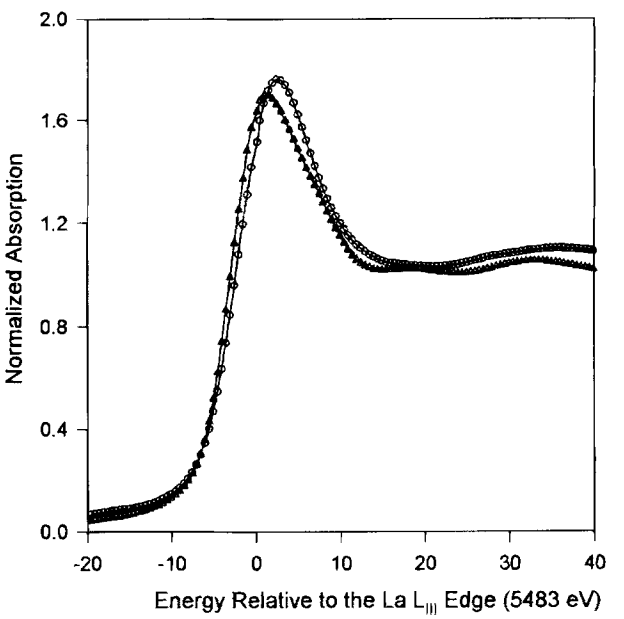

Fig. 13. Comparison of *in situ* La L_{III} edge spectra for $LaNi_5$ as a function of state of charge. $LaNi_5$ charged (○) and discharged (△).

(IV). The present results indicate that in the unhydrided alloy the Ce is in an α-like configuration similar to that found for $CeNi_5$. [32] On charging, the Ce becomes γ-like. Capehart *et al.* have done XAS studies on Ce_2Fe_{17}, $Ce_2Fe_{14}B$, and $CeFe_{14}BH_x$ alloys and concluded that the volume of the rare earth site was the principal factor controlling the electronic configuration about the Ce, with an expanded lattice favoring γ-like Ce. [34] Hence lattice expansion as a result of hydriding causes the α-like Ce to convert to the γ-form. The XANES results for the discharged electrode after 25 cycles indicates that there is some corrosion of Ce. The predominance of the low energy peak indicates that the corrosion product is largely trivalent Ce.

Conclusions

This study clearly demonstrates that *in situ* XAS is a very useful tool for the study of complex metal hydride materials since it provides both electronic and structural information. The element-specific nature of the probe makes it very useful for elucidating the role of minor constituents and the corrosion of individual components.

1. The XRD analysis result shows that the effect of substitution of Ni by Sn causes an increase in the lattice parameters primarily along the *c* axis. This manifests itself in a corresponding increase in the unit cell volume. Substitution of La by Ce, however, causes a minor contraction in the cell volume.
2. The XANES results at the Ni K edge indicates that the alloying process results in hybridization of the 4p and 3d orbitals of Ni. The addition of Sn and Ce apparently decreases the number of Ni d band vacancies. This could account for both the decreased hydrogen content and the reduced plateau pressure.
3. All of the XANES results at the Ni K and the La L_3 edge support the theoretical calculations of Gupta for $LaNi_5$ and $LaNi_5H_7$. [30]

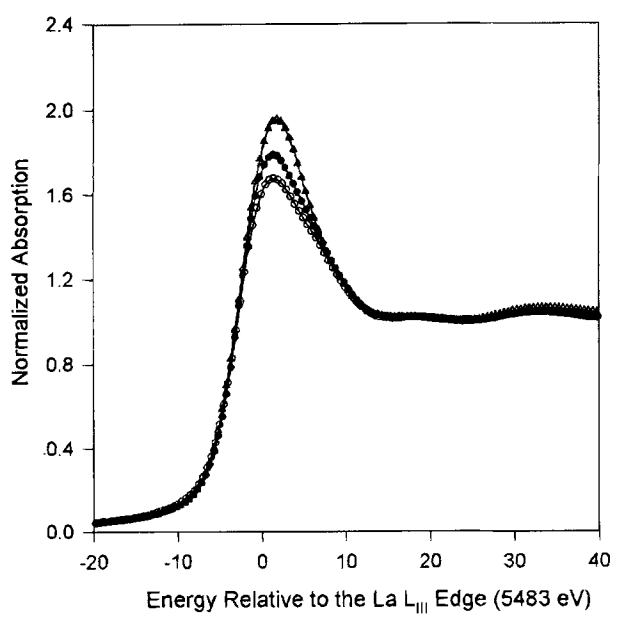

Fig. 12. Comparison of the La L_{III} edge XANES for $LaNi_5$ (○), $LaNi_{4.8}Sn_{0.2}$ (●), and $La_{0.8}Ce_{0.2}Ni_{4.8}Sn_{0.2}$ (△) in dry uncharged electrodes.

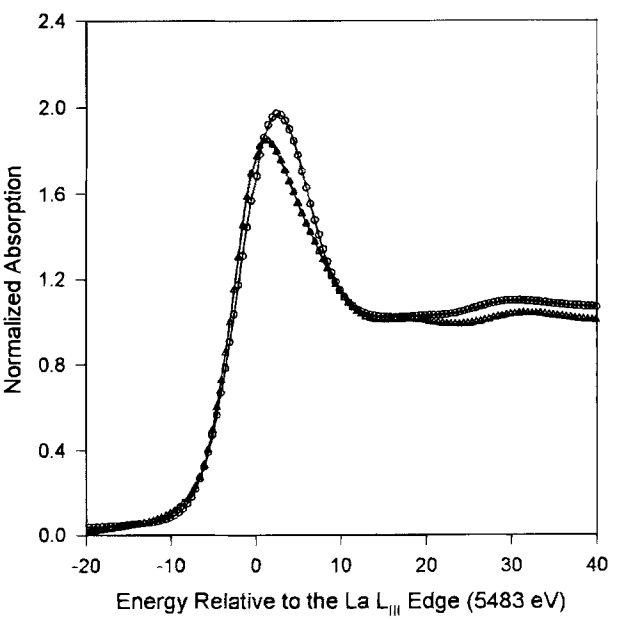

Fig. 14. Comparison of *in situ* La L_{III} edge spectra for $LaNi_{4.8}Sn_{0.2}$ as a function of state of charge. $LaNi_{4.8}Sn_{0.2}$ charged (○) and discharged (△).

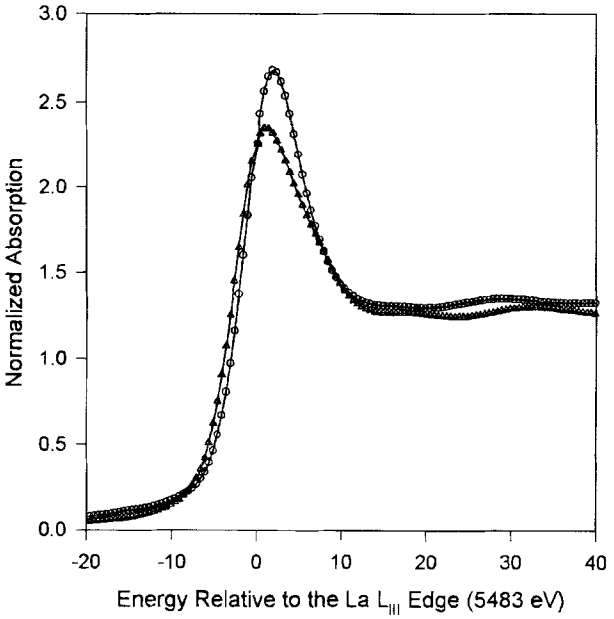

Fig. 15. Comparison of *in situ* La L_{III} edge spectra for $La_{0.8}Ce_{0.2}Ni_{4.8}Sn_{0.2}$ as a function of state of charge. $La_{0.8}Ce_{0.2}Ni_{4.8}Sn_{0.2}$ charged (○) and discharged (△).

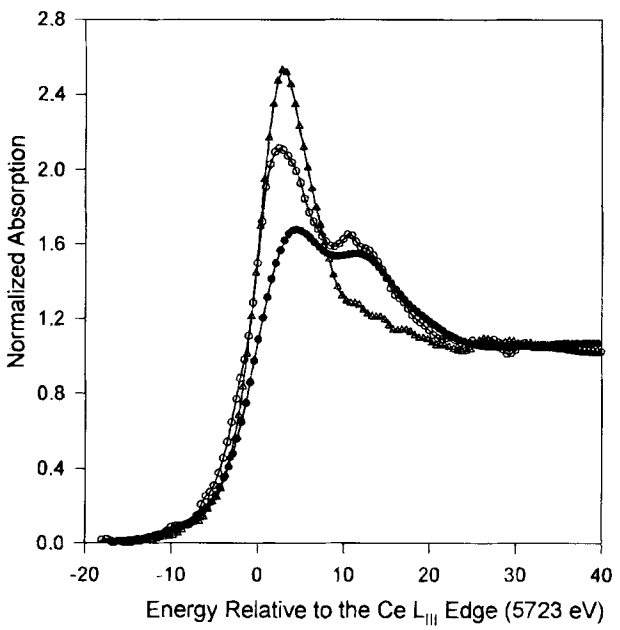

Fig. 16. Comparison of Ce L_{III} edge spectra for $La_{0.8}Ce_{0.2}Ni_{4.8}Sn_{0.2}$ as a function of state of charge and cycling. $La_{0.8}Ce_{0.2}Ni_{4.8}Sn_{0.2}$ dry uncharged (●), *in situ* charged (△), and dry *ex situ* discharged (○) after 25 cycles.

4. Both XANES and EXAFS confirm that about 6% of the Ni in $La_{0.8}Ce_{0.2}Ni_{4.8}Sn_{0.2}$ corrodes after 25 cycles.

5. XANES results at the Ce L_3 edge indicate that hydriding causes Ce to convert from an α- to a γ-like state. Results on cycled electrodes indicate corrosion of Ce with a predominance of Ce (III) in the corrosion product.

Acknowledgments

This work was performed under the auspices of the U. S. Department of Energy, Division of Chemical Sciences, Office of Basic Energy Science, under Contract No. DE-AC02-76CH00016. We would like to acknowledge the support the Department of Energy, Division of Material Science, Brookhaven National Laboratory (Contract No. DE-AC02-76CH00016) for its role in the development and operation of the National Synchrotron Light Source (NSLS). The help of personnel at the Beam Line X23A2 in particular Joe Woicik and John Kirkland, and Geraldine Lamble at the X11A Beam Line, is gratefully acknowledged.

Manuscript submitted Sept. 28, 1994; revised manuscript received March 21, 1995.

Brookhaven National Laboratory assisted in meeting the publication costs of this article.

REFERENCES

1. J. J. Reilly, in *Hydrogen Storage Materials, Batteries and Electrochemistry,* D. A. Corrigan and S. Srinivasan, Editors, PV 92-5, p. 24, The Electrochemical Society Proceedings Series, Pennington, NJ (1992).
2. A. Anani, A. Visintin, S. Srinivasan, A. J. Appleby, and H. S. Lim, *This Journal,* **137,** 985 (1992).
3. M. P. S. Kumar, K. Petrov, W. Zhang, A. A. Rostami, S. Srinivasan, G. Adzic, J. R. Johnson, J. J. Reilly, and H. S. Lim, Abstract 790, p. 1225, The Electrochemical Society Extended Abstracts, Vol. 94-1, San Francisco, CA, May 22-27, 1994.
4. M. Gupta and L. Schlapbach, *Hydrogen in Intermetallic Compounds I, Topics in Physic Series,* Vol. 63, S. Schlapbach, Editor, p. 139, Springer Verlag, New York (1988).
5. K. Tanaka, C. Sugiura, S. Nakai, and Y. Ohno, *Jpn. J. App. Phys.,* **20-1,** 41 (1981).
6. B. Lengeler and R. Zeller, *J. Less Common Met.,* **103,** 337 (1984).
7. J. Garcia, J. Bartolome, and M. S. del Rio, *Zeitschrift fur Physikalische Chemie Nue Folge, Bd.,* **163,** S. 277 (1989).
8. T. Suenobu, H. Sakaguchi, T. Tsuji, H. Kanai, S. Yoshida, and G. Adachi, *Bull. Chem. Soc. Jpn.,* **64,** 3522 (1991).
9. T. Suenobu, H. Sagakuchi, G. Adachi, H. Kanai, and S. Yoshida, *J. Alloys Compounds,* **190,** 273 (1993).
10. D. A. Tryk, I. T. Bae, Y. Hu, S. Kim, M. R. Antonio, and D. A. Scherson, *This Journal* **142,** 824 (1995).
11. J. J. Reilly and R. H. Wiswall, *Inorg. Chem.,* **9,** 1968, (1970).
12. G. D. Adzic, J. R. Johnson, J. J. Reilly, J. McBreen, S. Mukerjee, M. P. S. Kumar, W. Zhang, S. Srinivasan, and K. Petrov, in *Proceedings of the Symposium on Electrochemistry and Material Science of Cathodic Hydrogen Absorption and Adsorption,* B. E. Conway and G. Jerkiewicz, Editors, PV 94-21, p. 104, The Electrochemical Society Proceedings Series, Pennington, NJ (1994).
13. J. McBreen, W. E. O'Grady, K. I. Pandya, R. W. Hoffman, and D. E. Sayers, *Langmuir,* **3,** 418, (1987).
14. S. Mukerjee, S. Srinivasan, M. P. Soriaga, and J. McBreen, *This Journal,* **142,** 1409, (1995).
15. K. I. Pandya, R. W. Hoffman, J. McBreen, and W. E. O'Grady, *ibid.,* **137,** 383 (1990).
16. J. J. Reilly, in *Inorganic Synthesis,* S. L. Holt, Editor. p. 90, John Wiley & Sons, Inc., New York (1983).
17. M. H. Mendelsohn, D. M. Gruen, and A. E. Dwight, *ibid.,* p. 96.
18. D. E. Sayers and B. A. Bunker, in *X-ray Absorption: Principles, Applications, Techniques of EXAFS, SEXAFS and XANES,* D. C. Koningsberger and R. Prins, Editors, p. 211, John Wiley & Sons, Inc., New York (1988).
19. J. Wong, F. W. Lyttle, R. P. Messner, and D. H. Maylotte, *Phys. Rev. B,* **30,** 5596 (1984).
20. J. B. A. D. vanZon, D. C. Koningsberger, H. F. I. vant'Blik, and D. E. Sayers, *J. Chem. Phys.,* **82,** 5742 (1985).
21. F. B. M. Duivenvoorden, D. C. Koningsberger, Y. S. Oh, and B. C. Gates, *J. Am Chem. Soc.,* **108,** 6254 (1986).
22. K. I. Pandya, W. E. O'Grady, D. A. Corrigan, J. McBreen, and R. W. Hoffman, *J. Phys. Chem.,* **94,** 21 (1990).
23. M. Varrkamp, I. Dring, R. J. Oldman, E. A. Stern, and D. C. Koningsberger, *Phys. Rev. B,* **50,** 7872 (1994).
24. P. H. Citrin, P. Eisenberger, and B. M. Kincaid, *Phys. Rev. Lett.,* **36,** 1346 (1976).
25. J. J. Rehr, J. Mustre de Leon, S. I. Zabinski, and R. C. Albers, *J. Am. Chem. Soc.,* **113,** 5135 (1991).
26. B. V. Rathnakumar, C. Withman, B. Fultz, and G. Halpert, *This Journal,* **141,** L89 (1994).
27. P. Thompson, J. J. Reilly, L. M. Corliss, J. M. Hastings, and R. Hempelmann, *J. Phys. F: Met. Phys.,* **16,** 675 (1986).

28. J. S. Cantrell. T. A. Beiter, and R. C. Bowman, Jr., *J. Alloys Comp.*, **207-208,** 372 (1994).
29. A. N. Mansour, C. A. Melendres, M. Pankuch, and R. A. Brizzolara, *This Journal,* **141,** L69 (1994).
30. M. Gupta, *J. Less Common Met.*, **130,** 219 (1987).
31. D. C. Kosenmaki and K. A. Gschneidner, Jr., *Handbook on the Physics and Chemistry of Rare Earths,* K. A. Gschneidner, Jr., and L. Eyring, Editors, pp. 337-377, North Holland, Amsterdam (1978).
32. D. Wohllenben and J. Rohler, *J. Appl. Phys.*, **55,** 1904 (1984).
33. G. Krill, *J. Phys. C,* **8,** 907 (1986).
34. T. W. Capehart, R. W. Mishra, G. P. Meisner, C. D. Fuerst, and I. F. Herbgst, *Appl. Phys. Lett.*, **63,** 3642 (1993).
35. J. J. G. Willems, *Phillips J. Res.*, **39,** 1 (1984).

Improvements in Fluorine Generation: Amorphous Carbon Anodes with Vertical Channels

W. V. Childs and G. L. Bauer

3M Fluorochemical and Process Technology Center, St. Paul, Minnesota 55144-1000, USA

ABSTRACT

We describe improvements that have allowed us to operate fluorine cells with YBD® amorphous carbon anodes for over 2000 h and at current densities over 200 mA · cm^{-2} practically free of polarization. Vertical channels, 0.2 mm wide and 2 mm deep, facilitate the movement of fluorine up the face of the anode to the electrolyte surface where it escapes into the vapor space. One anode was operated at 226 mA · cm^{-2}; it polarized at 100 h, was subjected to a high voltage treatment, and then ran for over 2000 h without polarizing. Another anode ran well at 338 mA · cm^{-2}. Current efficiency estimates for hydrogen generation and for fluorine generation were near 100%.

Introduction

As shown in Fig. 1, within a few minutes of a fresh piece of carbon being made anodic the voltage required to pass 25 mA · cm^{-2} of current from molten KF · 2HF increased from about 3 V to over 5 V (at 12 min the current density was increased to a bit over 50 mA · cm^{-2}). At the same time, as shown in Fig. 2, the carbon surface changed from wetting (Fig. 2A), to highly nonwetting (Fig. 2B). These are irreversible changes. This is consistent with the reports of Bai and Conway,[1] Rudge,[2] and Brown *et al.*[3] that a very high contact angle leads to the formation of strongly adherent lenticular bubbles of fluorine that cover most of the anode surface. This behavior is ascribed to the formation of a layer of fluorinated carbon, CF_x, which is not wetted by the electrolyte and through which electrons must tunnel.

This coverage of the surface with bubbles makes it difficult for current to pass from the electrolyte into the anode surface and leads to what has been variously called an "anode effect," "polarization," and "aging." We follow Rudge[2] and call it polarization. It is characterized by a rather sudden increase in the cell voltage and, if the power supply voltage is limited to about 15 V (see below), by a decrease of current to a small fraction of the initial current. Barring drastic treatment this is an irreversible process.

In their first paper Bai and Conway[1a] concluded that "the formation and detachment of F_2 bubbles is the current-controlling factor for the fluorine evolution reaction at carbon anodes in the high current density range (i > 10 mA · cm^{-2})." Presumably wherever the current can work into the anode surface the local current density will be very high, and the local anode will be highly fluorinated and become even more nonwetting. Thus we have a feedback mechanism that will lead to more frequent polarization at higher current densities. In their third paper[1c] they reported extensively on a treatment that had been previously described by Rüdorf[4] and by Childs[5,6] and by Childs and Ruehlen.[7] It is a high voltage treatment that appears to be rather drastic but it is straightforward, can be carried out quickly and easily, and is effective (see below). Bai and Conway[1c] conclude that "[t]he improvements ... are believed to be associated mainly with facilitation of the detachment of the fluorine gas bubble/film..."

We have taken the view that the improvements from the high voltage treatment are mainly due to facilitation of the movement of bubbles up the surface without detachment. We have proposed and tested an anode design that further enhances this movement. That design provides for vertical channels up the face of the anode to collect the bubbles and facilitate their movement up the face. (Simple pressure drop calculations show that our channels, which are as narrow as our shops can reasonably make with a saw, would be adequate for fluorine generation rates perhaps an order of magnitude higher than we produce.) In this paper we describe this anode design that, in combination with the high voltage treatment, has allowed us to operate a fluorine generating carbon anode in KF · 2HF for well over 2000 h at 226 mA · cm^{-2}. A similar anode was operated at 226 mA · cm^{-2} for over 1000 h and then at 338 mA · cm^{-2} for 132 h without trouble. Both anodes were in excellent condition when the runs were stopped.

A control anode of YBD carbon without channels polarized and was depolarized at 50 h and at 200 h at 226 mA · cm^{-2}. Polarization of these anodes was intolerably frequent at higher current densities.

We also describe a simple method for estimating the current efficiencies for hydrogen generation and for fluorine generation. These estimates are near 100%.

Making Fluorine

Caution: The procedures described in this paper pose the risk of exposure to hydrogen fluoride and to elemental fluorine and should only be carried out by or under the direction of qualified professionals. Hydrogen fluoride and fluorine are dangerous materials. Exposure to them may cause severe, painful, and perhaps fatal burns. This exposure may not be evident for several hours. Qualified first aid treatment and professional medical resources must be established prior to working in the area. Prompt treatment is necessary to reduce the severity of damage from exposure and should be sought immediately following exposure or suspected exposure. Material Safety Data Sheets are available from HF and fluorine suppliers. The recommendations contained therein should be followed scrupulously. The Appendix should be referred to for some useful, perhaps essential, suggestions about experimental procedures and techniques.